



**HAL**  
open science

## An improved setup for radial diffraction experiments at high pressures and high temperatures in a resistive graphite-heated diamond anvil cell

Julia Immoor, Hauke Marquardt, Lowell M Miyagi, S. Speziale, Sébastien Merkel, I. Schwark, A. Ehnes, Hanns-Peter Liermann

### ► To cite this version:

Julia Immoor, Hauke Marquardt, Lowell M Miyagi, S. Speziale, Sébastien Merkel, et al.. An improved setup for radial diffraction experiments at high pressures and high temperatures in a resistive graphite-heated diamond anvil cell. *Review of Scientific Instruments*, 2020, *Review of Scientific Instruments*, 91 (4), pp.045121. 10.1063/1.5143293 . hal-02558603

**HAL Id: hal-02558603**

**<https://hal.univ-lille.fr/hal-02558603v1>**

Submitted on 29 Apr 2020

**HAL** is a multi-disciplinary open access archive for the deposit and dissemination of scientific research documents, whether they are published or not. The documents may come from teaching and research institutions in France or abroad, or from public or private research centers.

L'archive ouverte pluridisciplinaire **HAL**, est destinée au dépôt et à la diffusion de documents scientifiques de niveau recherche, publiés ou non, émanant des établissements d'enseignement et de recherche français ou étrangers, des laboratoires publics ou privés.

1 An improved setup for radial diffraction experiments at high  
2 pressures and high temperatures in a resistive graphite-heated  
3 diamond anvil cell.

4 J. Immoor<sup>1</sup>, H. Marquardt<sup>2</sup>, L. Miyagi<sup>3</sup>, S. Speziale<sup>4</sup>, S. Merkel<sup>5</sup>, I. Schwark<sup>6</sup>, A. Ehnes<sup>6</sup>, H.-  
5 P. Liermann<sup>6</sup>

6 <sup>1</sup>Bayerisches Geoinstitut BGI, University of Bayreuth, 95440 Bayreuth, Germany;

7 <sup>2</sup>Department of Earth Sciences, University of Oxford, Oxford OX1 3AN, UK; <sup>3</sup>University of

8 Utah, 115 So. 1460 E., Salt Lake City, UT84112-0111, USA; <sup>4</sup>German Research Center for

9 Geosciences GFZ, 14473 Potsdam, Germany; <sup>5</sup>Univ. Lille, CNRS, INRAE, Centrale Lille,

10 UMR 8207 - UMET - Unité Matériaux et Transformations, F-59000 Lille, France; <sup>6</sup>Photon

11 Sciences, Deutsches Elektronen-Synchrotron (DESY), 22607 Hamburg, Germany

12 \*Correspondence to: Julia.immoor@uni-bayreuth.de

13

14 Abstract

15 We present an improved setup for the experimental study of deformation of solids at  
16 simultaneous high pressures and temperatures by radial X-ray diffraction. The technique  
17 employs a graphite resistive heated Mao Bell type diamond anvil cell (DAC) for radial X-ray  
18 diffraction in combination with a water-cooled vacuum chamber. The new chamber has been  
19 developed by the sample environment group at PETRA III and implemented at the Extreme  
20 Conditions Beamline (ECB) P02.2 at PETRA III, DESY (Hamburg, Germany). We discuss  
21 applications of the new setup to study deformation of a variety of materials, including  
22 ferropericlase, calcium perovskite, bridgmanite, and tantalum carbide at high-  
23 pressure/temperature.

24

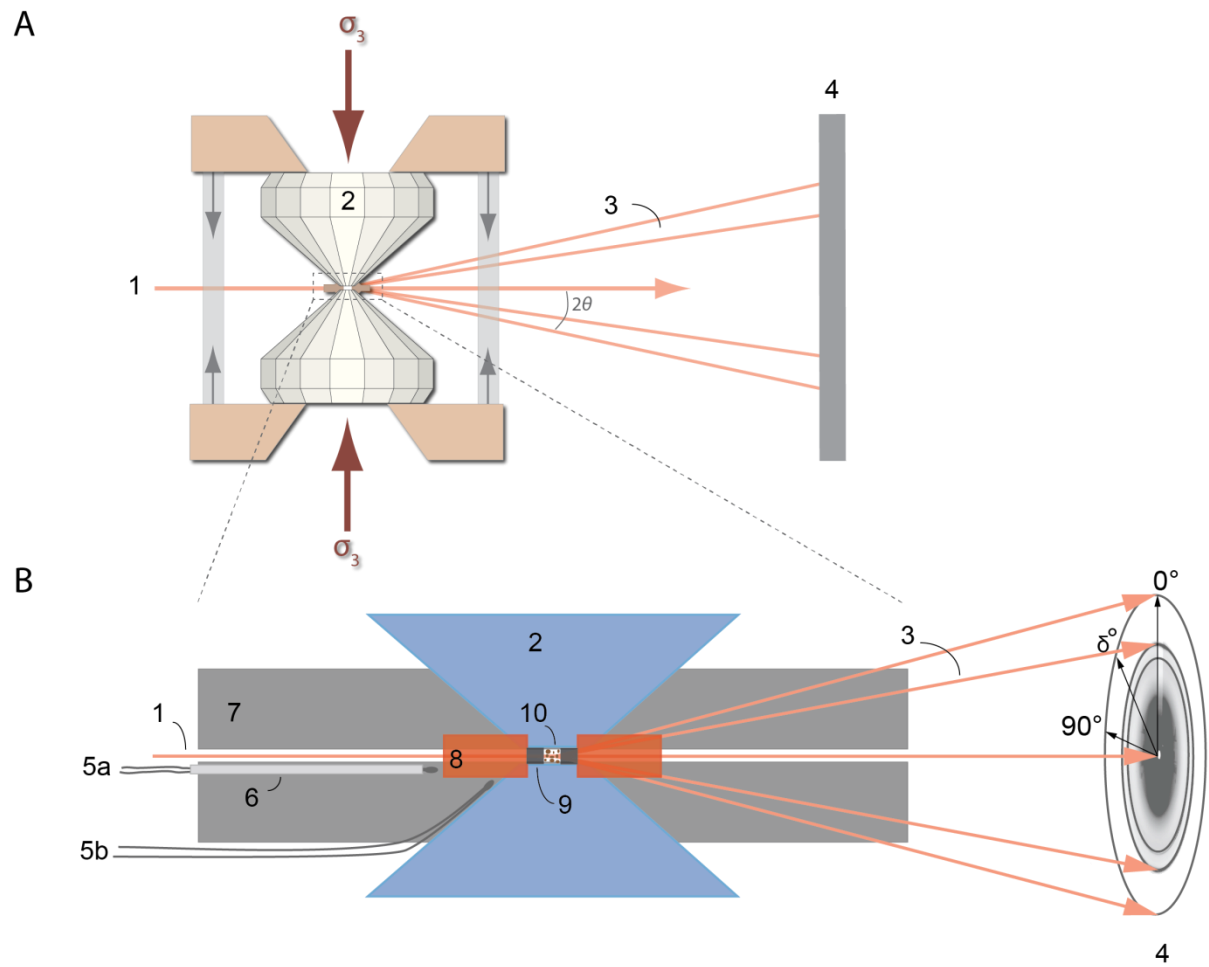
25 Introduction

26 Understanding the physical and rheological properties of materials at simultaneous high  
27 pressures and temperatures is of key importance in Earth science as well as materials sciences.

28 The rheological properties of Earth's mantle materials, for example, govern large-scale mantle  
29 convection<sup>1-4</sup>. In addition, Crystallographic Preferred Orientation (CPO) caused by the  
30 alignment of mantle minerals during deformation, leads to seismic anisotropy, providing a  
31 means to link seismic observations to mantle flow<sup>5-13</sup>. Several techniques have been  
32 developed in the past to study the rheology of materials under high pressure and temperature,  
33 but achievable pressures are mostly limited to those typical of the crust and upper mantle<sup>3,14-</sup>  
34 <sup>18</sup>.

35 Deformation experiments at deep lower mantle pressures are almost exclusively performed in  
36 diamond-anvil cells in combination with synchrotron-based in-situ X-ray diffraction in a  
37 radial geometry (Fig. 1A, B). By employing radial diffraction geometry, lattice strains and  
38 deviatoric stress as well as evolution of CPO can be derived from analysis of in situ  
39 diffraction images. Radial X-ray diffraction in DACs has been widely employed in Earth as  
40 well as materials sciences, but high-pressure experiments have been mostly limited to room  
41 temperature<sup>19-25</sup>. Early high-temperature employed a laser-heated DAC, but data analysis and  
42 interpretation is challenging due to temperature gradients in the sample<sup>26,27</sup>. Liermann *et al.*,  
43 (2009)<sup>28</sup> developed a resistive-heated DAC, which was tested up to 36 GPa and 1100 K while  
44 performing in-situ radial X-ray diffraction. The use of a resistive-heating setup reduces  
45 temperature gradients and provides more homogeneous heating of the entire sample chamber.

This is the author's peer reviewed, accepted manuscript. However, the online version of record will be different from this version once it has been copyedited and typeset.  
PLEASE CITE THIS ARTICLE AS DOI:10.1063/1.5143293

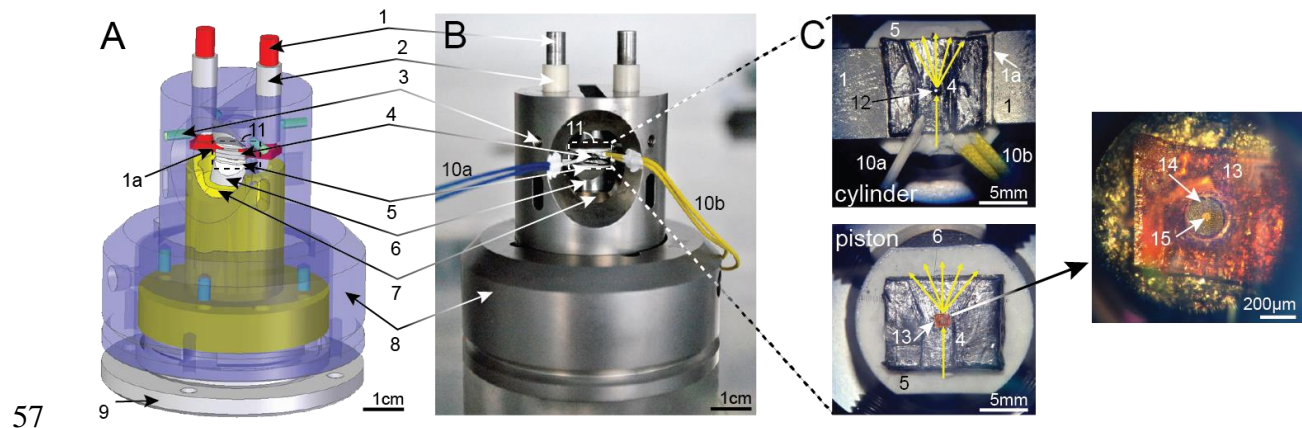


46

47 Figure 1: (A) angle-dispersive high-pressure radial X-ray diffraction in a DAC (modified after  
48 <sup>28</sup>);  $\sigma_3$ : stress along compression direction;  $2\theta$ : diffraction angle; 1: incoming X-ray Beam; 2:  
49 Diamond anvil; 3: Diffracted beam; 4: Area detector. (B) Magnification of the diamond-anvil  
50 culets showing the position for the two thermocouples (5a: between both graphite heaters; 5b:  
51 on the diamond anvil next to the culet). 6: Ceramic sleeve; 7: Flexible graphite sheet; 8:  
52 Kapton; 9: Boron gasket; 10: sample.

53

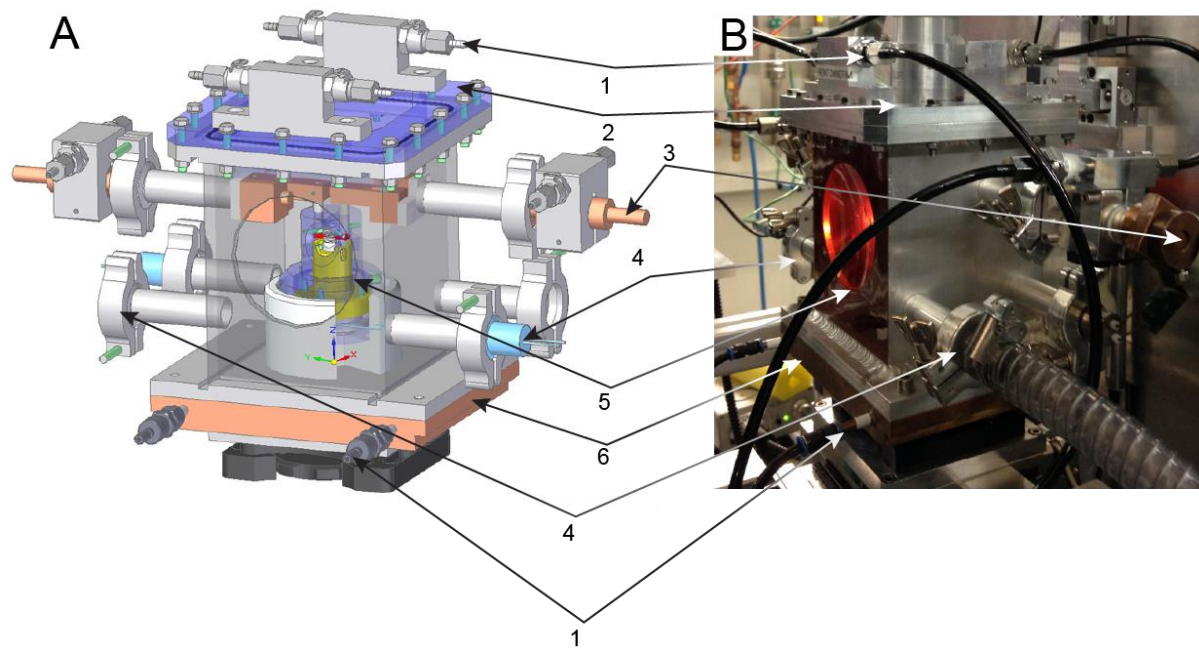
54 Here, we present a modified resistive-heated-radial-X-ray-diffraction-diamond-anvil-cell  
55 (RH-rXRD-DAC) (Fig. 2A, B) and report on its performance during in-situ radial X-ray  
56 diffraction experiments at simultaneous high pressure and high temperature on several



57  
58 Figure 2: Experimental setup of a resistive-heated DAC (modified after<sup>10</sup>). (A) 3D CAD  
59 model and (B) photograph of the resistive-heated DAC used for the experiments. 1:  
60 Molybdenum rods (electrical contacts); 1a: Strip with step at the end of molybdenum rod; 2:  
61 Ceramic sleeves; 3: Screws; 4: Graphite sheet; 5: Ceramic plate; 6: Tungsten carbide seat; 7:  
62 Piston; 8: Cylinder; 9: Membrane cup (missing in B); 10a: Thermocouple with ceramic  
63 sleeve; 10b: Thermocouple; 11: Graphite-heater. (C) Close-up of 11. Cylinder: 12: Culet of a  
64 diamond; 4: Flexible graphite sheet with carved space for X-ray beam. Inset shows the lower  
65 diamond pressed into the graphite heater and illustrates the positions of the thermocouples.  
66 Piston: 13: Kapton, which supports a cubic boron nitride gasket or amorphous boron epoxy  
67 gasket (14) with powder sample in the sample chamber (15).

68  
69 polycrystalline samples. The main improvement as compared to the setup described by  
70 Liermann et al. (2009) is the development and implementation of a water-cooled vacuum  
71 chamber (Fig. 3A, B) that also enables cooling of the piston of the Mao Bell type DAC. This  
72 modification decreases heating and thermal expansion of the piston of the Mao Bell DAC but  
73 allows the cylinder to heat up, thus reducing friction between the piston and the cylinder  
74 during compression at high temperatures. The use of a vacuum chamber prevents the  
75 oxidation of the cell, the Molybdenum rods and the diamonds at very high temperatures. We

76 discuss applications of the improved setup for studying the deformation behavior of major  
77 materials expected in Earth's lower mantle as well as tantalum carbide.



78  
79 Figure 3: (A) 3D CAD model of the vacuum chamber. (B) Photograph of the vacuum  
80 chamber while performing a high-temperature experiment ( $\sim 1400$  K). 1: Water cooling  
81 inlet/outlet; 2: Lid with screws; 3: Power supply connector; 4: Vacuum pump connection; 5:  
82 Kapton window; 6: Copper cooling plate.

83

#### 84 Experimental Method

85 In radial X-ray diffraction experiments, the incoming X-ray beam is oriented perpendicular to  
86 the compression direction, i.e. the axis of the diamond anvils (Fig. 1A, C: 1). This setup  
87 provides the possibility to study the lattice strains, resulting from the effect of differential  
88 stress, together with the CPO of powder samples<sup>19</sup>. A pressure-transmitting medium is not  
89 used. This enhances the development of differential stress and texture. In order for X-rays to  
90 reach the sample chamber in the radial diffraction geometry, X-ray transparent gaskets are  
91 required. Here, we used either X-ray transparent amorphous boron epoxy + kapton<sup>29</sup> or cubic  
92 boron nitride (cBN) epoxy<sup>27</sup> (10:1 Epotech 353ND) + kapton gaskets (Fig. 1: 8, 9; Fig. 2C:

93 13, 14) to reach high pressures<sup>30</sup>. The culet sizes of the employed diamonds were 200  $\mu\text{m}$  or  
94 300  $\mu\text{m}$  (Fig. 2C: 12). The setup of the graphite heater is similar on the piston and cylinder  
95 side of the DAC (Fig. 2C). Diamonds are glued on tungsten carbide seats that are truncated at  
96 the side to increase the opening angle for diffracted X-rays (Fig. 2: 5). The seats are insulated  
97 from the graphite by a ceramic ring (Fig. 2: 4) fixed to the seat with OMEGABOND 500  
98 liquid. The gaps between the ceramic plates and the diamonds are filled with ceramic glue  
99 (Resbond 989). The heads of the molybdenum rods end in horizontal strips with a small step  
100 at the end. A piece of graphite foil connects the molybdenum rods (Fig. 2A: 1a; Fig. 2B: 11;  
101 Fig. 2C: 1a) and serves as heating element surrounding the diamond-anvils. A space is carved  
102 in the graphite foil to prevent diffraction of the graphite contaminating the diffraction image.  
103 Two thermocouples (R-type) are attached to the cylinder side. One thermocouple is placed  
104 close to the tip of the diamond on the upstream side of the DAC and to the side of the path of  
105 the incident X-ray beam (Fig 2C: 10a). The second thermocouple is positioned on the graphite  
106 sheet, likewise upstream and to the side of the incident X-ray beam (Fig. 2C: 10b). When the  
107 cell is closed, the second thermocouple rests between the graphite sheets of the piston and the  
108 cylinder.  
109 During the experiment, the temperature of the sample can be increased/decreased by varying  
110 an analog I/O signal from 0-10 V using the beamline control system. This proportionally  
111 adjusts the power of the DC power supply from 0-1800 W (0–8 V and 0–220 A)<sup>31</sup>. Pressure  
112 is changed remotely using a gas membrane device that is operated by the membrane pressure  
113 controller APD200 from Sanchez Technology<sup>27,28,32</sup>.  
114 For high-pressure and high-temperature experiments, the RH-rXRD-DAC is placed in a  
115 newly-designed water-cooled vacuum chamber that serves to both cool the DAC and to  
116 prevent oxidation of the DAC, the molybdenum electrodes, the diamond anvils and the  
117 graphite heater (Fig. 3A, B). The piston of the DAC is indirectly cooled through a steel pin

118 that is connected to the base of the vacuum chamber, which is water-cooled. The differential  
119 cooling between the piston and the cylinder reduces the friction between the two parts of the  
120 DAC and enables a smoother pressure increase as compared to the previous experimental  
121 setup<sup>27,28</sup>. During the experiment the vacuum in the chamber can be as good as  $5 \times 10^{-3}$  mbar.  
122 Note that, due to connections between the pump and the cell chamber, vacuum levels around  
123 the diamond anvil cells may not be as efficient. Nevertheless, the achieved vacuum is  
124 sufficient to perform experiments with minimal oxidation of the heating elements.

125

126 Results and discussion

127 The new setup has been tested during different experimental campaigns at the ECB P02.2 at  
128 PETRA III, DESY (Hamburg, Germany). Diffraction images were collected with a XRD  
129 1621 flat panel detector from Perkin Elmer. In the following, we will describe some selected  
130 experiments in order to illustrate the capability of the new setup for Earth and materials  
131 science research. We report on the deformation of polycrystalline samples of ferropericlasite  
132 ( $(\text{Mg}_{0.8}\text{Fe}_{0.2})\text{O}$ ), the in-situ synthesis and deformation of cubic Ca-Pv ( $\text{CaSiO}_3$ ), experiments  
133 performed on a two-phase mixture of bridgmanite ( $\text{MgSiO}_3$ ) and ferropericlasite, synthesized  
134 from a mixture of enstatite glass + ferropericlasite in the resistive-heated DAC, as well as the  
135 high-temperature compression of tantalum carbide ( $\text{TaC}_{0.99}$ ), an ultra-high temperature  
136 ceramic material.

137

138 *1. In-situ deformation of ferropericlasite*

139 Ferropericlasite is the second most abundant mineral in Earth's lower mantle. It may play a key  
140 role in mantle dynamics since it is rheologically weaker than bridgmanite, the dominant lower  
141 mantle phase. Furthermore, it shows a pronounced elastic anisotropy, making it one of the  
142 candidates to explain seismic shear wave polarization anisotropy in the lower mantle<sup>33</sup>.



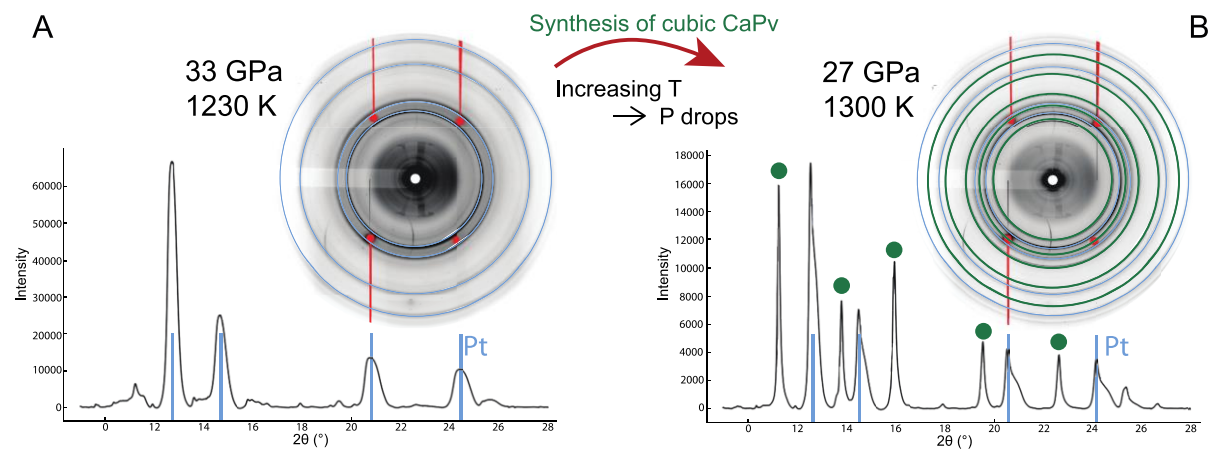
143 However, previous deformation studies at pressures of the lower mantle were limited to room  
144 temperature due to experimental complexity<sup>19,21–23,34,35</sup>. In Immoor *et al.* (2018), we used the  
145 described setup to measure the deformation of ferropericlase to 62 GPa at 1400 K as well as  
146 to higher pressures but lower temperature. In our 1400 K run, the pressure of the sample was  
147 increased up to 40 GPa at room temperature and afterwards heated up to 1400 K. During  
148 heating, the pressure of the sample dropped to below 20 GPa. We increased the pressure again  
149 and reached 62 GPa when diamond failure stopped the experiment. During compression, we  
150 collected high quality diffraction images of ferropericlase. Based on these results, we were  
151 able to monitor the evolution of CPO in ferropericlase and confirm a change of slip system  
152 activity at high temperature as predicted by computations<sup>10</sup>.

153

## 154 2. *In-situ synthesis and deformation of cubic CaSiO<sub>3</sub>*

155 CaSiO<sub>3</sub> perovskite is expected to be an important mineral in Earth's transition zone and lower  
156 mantle, where it is the third most abundant phase for a pyrolytic mantle composition<sup>36</sup>. In a  
157 deeply subducted oceanic slab, CaSiO<sub>3</sub> perovskite may account for up to 25 Vol.% of the  
158 transformed basaltic crust<sup>37</sup> and will affect the bulk rheological properties of the lithospheric  
159 slab. According to a recent computational study<sup>38</sup>, the shear wave anisotropy of CaSiO<sub>3</sub>  
160 perovskite is about 15-30% at conditions of the lower mantle. A strong CPO of CaSiO<sub>3</sub>  
161 perovskite may, therefore, contribute to seismic anisotropy observations, in particular in the  
162 shallow lower mantle or lowermost transition zone, where the elastic anisotropy is strongest.  
163 A previous CaSiO<sub>3</sub> perovskite study has been limited to 49 GPa at ambient conditions<sup>23</sup>. At  
164 these conditions, however, CaSiO<sub>3</sub> perovskite forms a pseudo cubic structure and the exact  
165 nature of the distortion is still under debate<sup>39–42</sup>. Whereas at temperatures typical for the lower  
166 mantle, the structure is cubic (*Pm3m*)<sup>40–43</sup> and may show a different rheological behavior.  
167 CaSiO<sub>3</sub> perovskite can be experimentally synthesized from CaSiO<sub>3</sub> wollastonite at pressures

168 of about 20 GPa and temperature of about 1300 K<sup>44</sup>, but is not quenchable to ambient  
169 conditions. This implies that studies of the physical properties of CaSiO<sub>3</sub> perovskite need to  
170 be performed in-situ and in the same pressure device where it has been synthesized.  
171 Using the improved RH-rXRD-DAC, we were able to synthesize CaSiO<sub>3</sub> perovskite and  
172 performed several successful deformation experiments reaching temperatures of up to 1500 K  
173 at pressures of 45 GPa (Immoor *et al.* in prep.). The starting material was amorphous CaSiO<sub>3</sub>  
174 mixed with platinum powder as pressure standard. Figure 4 shows two diffraction images  
175 collected during a compression experiment that reached a final pressure of 40 GPa at 1300 K.  
176 Cubic CaSiO<sub>3</sub> perovskite was synthesized after increasing the temperature to 1300 K at which  
177 point the pressure dropped from 33 GPa to 27 GPa as a result of the phase transition (Fig.  
178 4B). The collected diffraction patterns show smooth diffraction rings, indicating a relatively  
179 small and homogeneous grain size of the synthesized cubic CaSiO<sub>3</sub> perovskite. The large  
180 pressure drop at the transition also caused strain heterogeneity in Pt finely mixed with the  
181 sample (see Pt peaks asymmetry in Fig. 4B).



182  
183 Figure 4: Synthesis of cubic calcium perovskite. The pressure was calculated from the  
184 stronger Pt peak. (A) X-ray diffraction image at 33 GPa and 1230 K shows rings of Pt (blue),  
185 which are used to estimate the pressure during the experiment and diamond single-crystal  
186 diffraction spots (red). The corresponding integrated diffraction pattern is shown below with

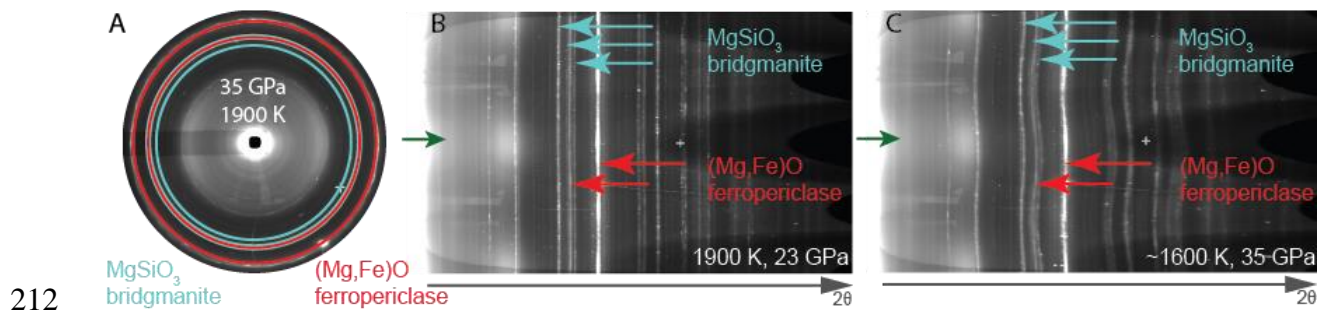
187 blue line indicating Pt peaks. (B) X-ray diffraction image at 27 GPa and 1300 K with Debye  
188 rings of Pt (blue), Debye rings of calcium perovskite (green) and diamond diffraction spots  
189 (red). At the bottom integrated diffraction pattern with blue lines indicating Pt peaks and  
190 green dots indicating calcium perovskite peaks.

191 In both panel (A) and (B) the diffraction lines of diamond are masked in the integration and  
192 absent in the diffraction patterns.

193

### 194 *3. Synthesis of Bridgmanite and Ferropericlase*

195 The deformation behavior of multiphase rock assemblies might substantially differ from the  
196 behavior of single-phase assemblies, particularly if the phases show large differences in  
197 rheological properties<sup>35,45–48</sup>. The lower mantle can be modeled as a two-phase mixture of  
198 bridgmanite and ferropericlase, two phases that show large differences in plastic strength and  
199 viscosity<sup>3,5,22</sup>. Because of this large contrast in rheological strength, it is difficult to predict  
200 mantle properties, including viscosity and seismic anisotropy, from single-phase  
201 measurements. There have been few deformation experiments on analogues<sup>49,50</sup>, as well as on  
202 a true two-phase lower mantle mixture at pressures and temperature of the very top of the  
203 lower mantle using a rational Drickamer apparatus<sup>3</sup>. Here, we used the improved RH-rXRD-  
204 DAC to synthesize a bridgmanite and ferropericlase assembly (Fig. 5A, B) from an enstatite  
205 glass powder mixed with ferropericlase, and applied deviatoric stress to the two-phase  
206 mixture at high temperatures (Fig. 5C). In one successful run, we first increased the pressure  
207 at 1600 K. Afterwards the pressure in the sample decreased while increasing the temperature  
208 continuously to 1900 K. A peak splitting of ferropericlase was observed, likely as a result of  
209 pressure gradients in the sample chamber, followed by the appearance of the typical  
210 diffraction ring triplet of the new phase bridgmanite. Bridgmanite grew while the pressure  
211 continued to decrease when the thermocouples stopped working. During a subsequent



212  
213 Figure 5: Synthesis of bridgmanite (blue) + ferropericlae (red). Green arrows indicate the  
214 compression direction in the unrolled radial X-ray diffraction image. (A) shows the  
215 diffraction rings of bridgmanite and ferropericlae at 35 GPa and 1900 K. (B) shows the  
216 unrolled image with the straight unrolled diffraction rings of bridgmanite and ferropericlae at  
217 23 GPa and 1900 K. (C) The unrolled diffraction image shows the curved unrolled diffraction  
218 rings of bridgmanite and ferropericlae after pressure increase up to 35 GPa at  $\sim 1600$  K.  
219 Ferropericlae was used as pressure calibrant.

220  
221 decrease of voltage and therefore presumably of temperature (based on power-temperature  
222 relation; see Fig. 6), the pressure in the sample chamber increased again to 35 GPa leading to  
223 deformation of the sample (Fig. 5C).

#### 224 225 4. Compression of tantalum carbide ( $TaC_{0.99}$ )

226 Carbides are characterized by high mechanical and thermal stability and play an important  
227 role in industrial applications, where they are used, for example, as coatings for abrasive  
228 tools. Many experimental and computational studies have been conducted on tantalum carbide  
229 (see references in<sup>51</sup>). However, no experiments have been performed to study the behavior of  
230 this phase under simultaneous high pressure, high temperature and deviatoric stress. We  
231 performed two successful experimental deformation runs on tantalum carbide ( $TaC_{0.99}$ ) and  
232 constrained the pressure-volume-temperature equation of state<sup>51</sup>. The starting material was

233 TaC<sub>0.99</sub> powder and the pressure was determined by a thin piece of Au foil (less than 5  $\mu\text{m}$ )  
234 using the EOS published in Fei et al. (2007). In the first run, we started heating when the  
235 pressure reached 2 GPa, we increased the temperature to 673 K, and measured X-ray  
236 diffraction up to a final pressure of 33 GPa along the 673 K isotherm. In the second run, we  
237 increased temperature at a pressure of  $\sim 2$  GPa up to 1073 K, and we collected X-ray  
238 diffraction images up to a final pressure of  $\sim 38$  GPa along an isothermal path. The data  
239 collected under non-hydrostatic conditions were used to constrain the quasi-hydrostatic high  
240 temperature EOS by extracting the hydrostatic unit-cell parameter from the x-ray diffraction  
241 data<sup>53</sup>. In addition these data can be used to determine the strength and activity of the slip  
242 systems of TaC<sub>0.99</sub> at simultaneous high-pressure and -temperature (Speziale *et al.* in prep.).

243

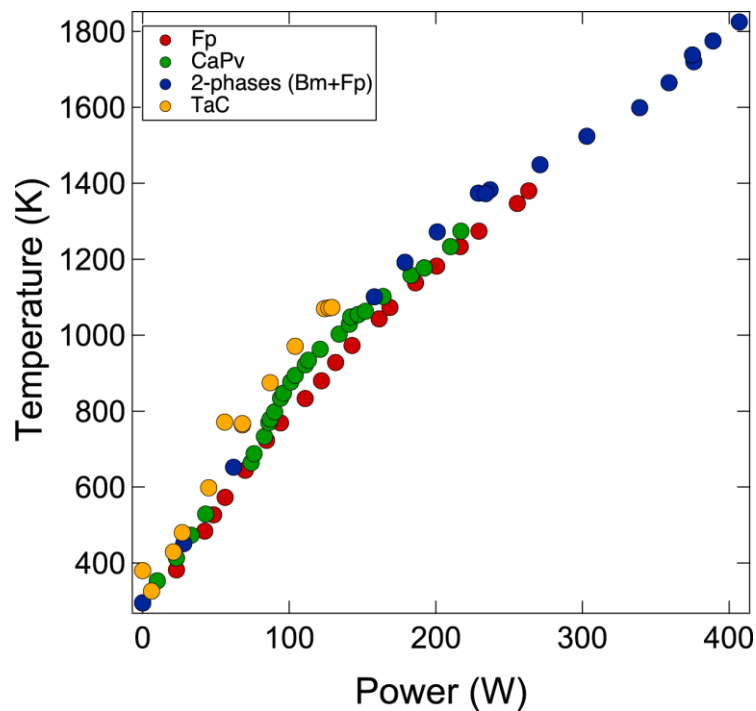
244 *5. Challenges and solutions*

245 In several experimental runs the DAC jammed during high-temperature experiments leading  
246 to discrete pressure jumps as opposed to smooth increases of pressure. Because of their  
247 brittleness the ceramic gaskets were not able to buffer these pressure jumps resulting in failure  
248 of the diamond anvils. The reason for our difficulties to smoothly increase pressure at very  
249 high temperatures could be the expansion of both the piston and the cylinder of the Mao Bell  
250 DAC leading to increased friction between both parts. However, at moderately high  
251 temperatures, up to 1400 K, the differential cooling was effective such that a smooth pressure  
252 increase is generally possible. For higher temperature experiments the indirect piston cooling  
253 is still insufficient, and needs to be improved in order to reduce the thermal expansion of the  
254 piston and thus the friction.

255 Using the water-cooled vacuum chamber, temperatures up to 1900 K have been reached in the  
256 RH-rXRD-DAC, but no pressure increase was possible. Generally, both thermocouples

257 recorded stable temperatures during the experiments, with a reproducible dependence of  
258 temperature on power (Fig. 6).

259 In a few runs, the difference in temperature reading between the two thermocouples was very  
260 large (the maximum difference observed was 400 K). In these cases higher temperature values  
261 were recorded by the thermocouple situated between the graphite sheets. Large differences in  
262 temperature reading usually occurred when one of the thermocouples, i.e. the one at the tip of  
263 the diamond was placed too far from the culet of the diamond.



264

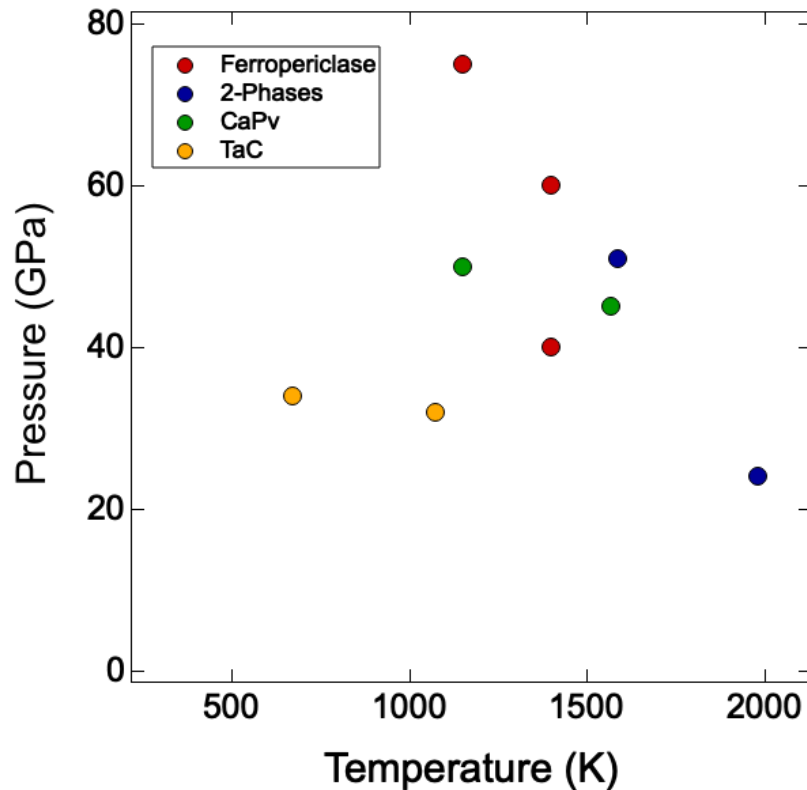
265 Figure 6: Power – Temperature curves of different experiments. The temperature is read using  
266 two thermocouples, one placed between the two graphite heaters and one placed on the  
267 diamond-anvil close to the sample. Symbols: Fp is ferropericlase; CaPv is calcium perovskite;  
268 Bm is bridgmanite; TaC is tantalum carbide.

269

270 Conclusion

271 We have presented an improved experimental setup for radial X-ray diffraction measurements  
272 based on a graphite-heated Mao Bell type diamond-anvil cell contained in a water-cooled

273 vacuum chamber. The setup is available for users at the Extreme Conditions Beamline P02.2  
274 at DESY, Hamburg and allows for reaching temperatures of up to 1900 K at high pressures  
275 (Fig. 7).



276  
277 Figure 7: Maximum pressure-temperature- conditions reached in experiments on  
278 ferropericlase (red, calculated pressure), 2-phases (enstatite (bridgmanite) + ferropericlase)  
279 (blue, estimated pressure), calcium perovskite CaPv (green, 45 GPa estimated pressure; 50  
280 GPa calculated pressure) and tantalum carbide TaC (yellow, calculated pressure) in different  
281 experimental runs.

282 Temperature and pressure in the diamond-anvil cell are controlled remotely during the  
283 experiment. Several successful experiments studies were performed by using the improved  
284 setup on a variety of Earth materials (ferropericlase, calcium perovskite, a two-phase  
285 bridgmanite-ferropericlase mixture) and tantalum carbide in order to show the capabilities of  
286 the resistive-heated-radial-X-ray-diffraction-diamond-anvil-cell. A major priority is currently

287 the search for a better gasket material which combines mechanical strength and high-  
288 temperature stability.

289

290 Acknowledgements

291 This research was supported through the projects “GeoMaX” funded under the Emmy-  
292 Noether Program of the German Science Foundation (MA4534/3-1) as well as grant  
293 MA4534/4-1. HM acknowledges support from the Bavarian Academy of Sciences. LM  
294 acknowledges support from the US Department of Energy, National Nuclear Security  
295 Administration, through the Capital-DOE Alliance Center (DE-NA0003858) and NSF (EAR-  
296 1344579 and EAR-1654687). SM acknowledges support from the Institut Universitaire de  
297 France and the program PNP of CNRS/INSU. We acknowledge DESY (Hamburg, Germany),  
298 a member of the Helmholtz Association HGF, for the provision of experimental facilities.  
299 Parts of this research were carried out at PETRA III and we would like to thank K. Glazyrin  
300 for assistance in using Beamline P02.2. Part of the research leading to this result has been  
301 supported by the project CALIPSO plus under the Grant Agreement 730872 from the EU  
302 Framework Programme for Research and Innovation HORIZON 2020.

303



304 References

305 <sup>1</sup> D.L. Kohlstedt, *Properties of Rocks and Minerals - Constitutive Equations, Rheological*  
306 *Behavior, and Viscosity of Rocks* (Elsevier B.V., 2007).

307 <sup>2</sup> N. Tsujino, Y. Nishihara, D. Yamazaki, Y. Seto, Y. Higo, and E. Takahashi, *Nature* 539, 81  
308 (2016).

309 <sup>3</sup> J. Girard, G. Amulule, R. Farla, A. Mohiuddin, and S. Karato, *Science*. 351, 144 (2016).

310 <sup>4</sup> S. Karato and P. Wu, *Science*. 260, 771 (1993).

311 <sup>5</sup> D. Yamazaki and S. Karato, *Am. Mineral.* 86, 385 (2001).

312 <sup>6</sup> B. Romanowicz and H.R. Wenk, *Phys. Earth Planet. Inter.* 269, 58 (2017).

313 <sup>7</sup> P.J. Tackley, *Science*. 288, 2002 (2000).

314 <sup>8</sup> S. Karato, *Phys. Earth Planet. Inter.* 51, 107 (1988).

315 <sup>9</sup> S. Karato, S. Zhang, and H.-R. Wenk, *Science*. 270, 458 (1995).

316 <sup>10</sup> J. Immoor, H. Marquardt, L. Miyagi, F. Lin, S. Speziale, S. Merkel, J. Buchen, A.  
317 Kurnosov, and H.P. Liermann, *Earth Planet. Sci. Lett.* 489, 251 (2018).

318 <sup>11</sup> N. Creasy, M.D. Long, and H.A. Ford, *J. Geophys. Res. Solid Earth* 122, 5243 (2017).

319 <sup>12</sup> C.P. Conrad, M.D. Behn, and P.G. Silver, *J. Geophys. Res. Solid Earth* 112, 1 (2007).

320 <sup>13</sup> A. Nowacki, A.M. Walker, J. Wookey, and J.M. Kendall, *Geophys. J. Int.* 192, 1085  
321 (2013).

322 <sup>14</sup> T. Kawazoe, N. Nishiyama, Y. Nishihara, T. Irifune, D. Suetsugu, C. Bina, T. Inoue, D.  
323 Wiens, and M. Jellinek, *Phys. Earth Planet. Inter.* 183, 190 (2010).

324 <sup>15</sup> Y. Wang, W.B. Durham, I.C. Getting, and D.J. Weidner, *Rev. Sci. Instrum.* 74, 3003  
325 (2003).

326 <sup>16</sup> D. Yamazaki and S.-I. Karato, *Rev. Sci. Instrum.* 72, 4207 (2001).

327 <sup>17</sup> T. Kawazoe, T. Ohuchi, Y. Nishihara, N. Nishiyama, K. Fujino, and T. Irifune, *Phys. Earth*  
328 *Planet. Inter.* 216, 91 (2013).

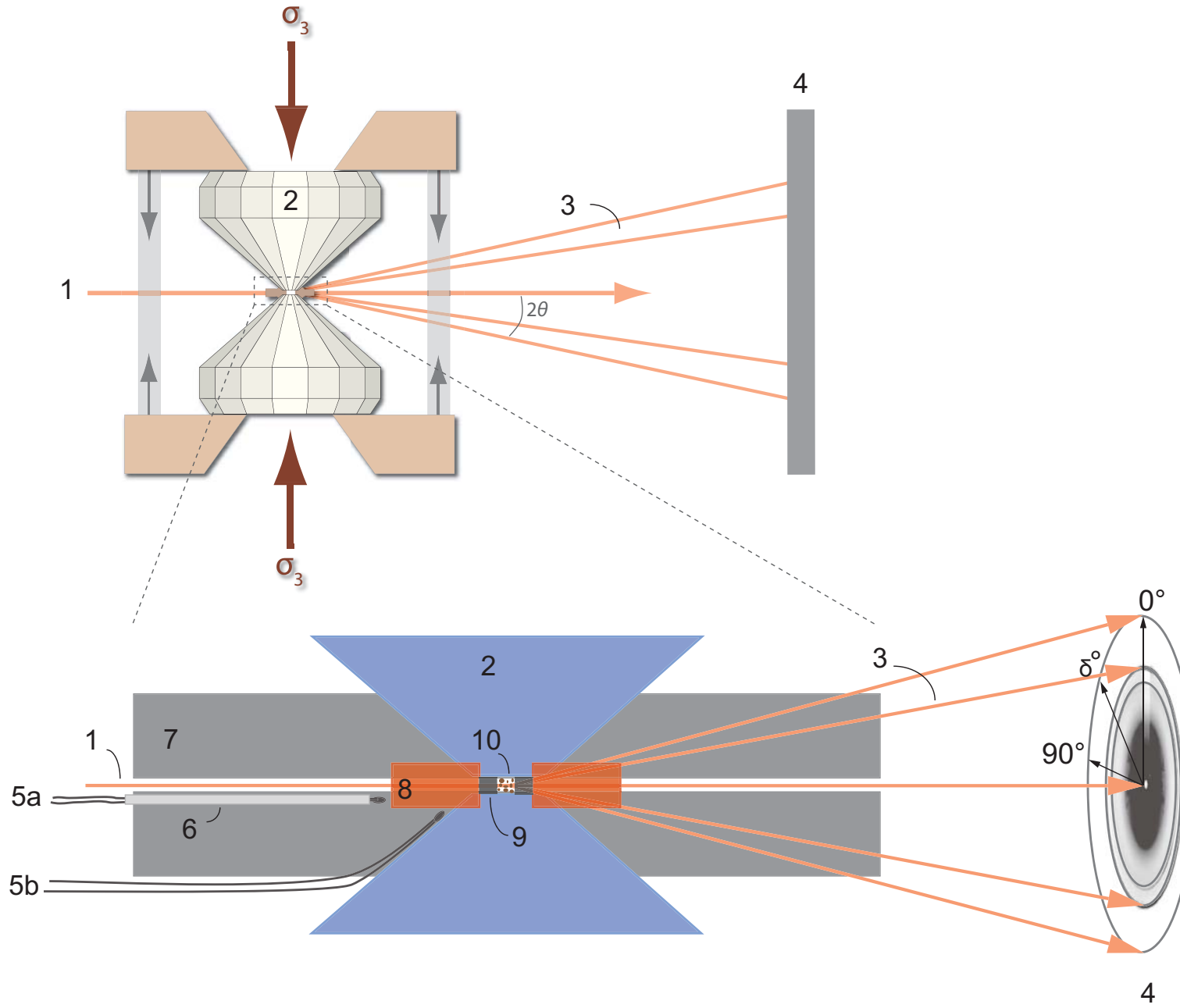
- 329 <sup>18</sup> S.A. Hunt and D.P. Dobson, *Rev. Sci. Instrum.* 88, (2017).
- 330 <sup>19</sup> H.-R. Wenk, I. Lonardelli, S. Merkel, L. Miyagi, J. Pehl, S. Speziale, and C.E. Tommaseo,  
331 *J. Phys. Condens. Matter* 18, S933 (2006).
- 332 <sup>20</sup> S. Merkel, *J. Phys. Condens. Matter* 18, S949 (2006).
- 333 <sup>21</sup> C.E. Tommaseo, J. Devine, S. Merkel, S. Speziale, and H.R. Wenk, *Phys. Chem. Miner.*  
334 33, 84 (2006).
- 335 <sup>22</sup> H. Marquardt and L. Miyagi, *Nat. Geosci.* 8, 311 (2015).
- 336 <sup>23</sup> L. Miyagi, S. Merkel, T. Yagi, N. Sata, Y. Ohishi, and H.R. Wenk, *Phys. Earth Planet.*  
337 *Inter.* 174, 159 (2009).
- 338 <sup>24</sup> H.-R. Wenk, J.R. Baumgardner, R.A. Lebensohn, and C.N. Tomé, *J. Geophys. Res. Solid*  
339 *Earth* 105, 5663 (2000).
- 340 <sup>25</sup> S. Merkel, A.K. McNamara, A. Kubo, S. Speziale, L. Miyagi, Y. Meng, T.S. Duffy, and  
341 H.R. Wenk, *Science*. 316, 1729 (2007).
- 342 <sup>26</sup> M. Kunz, W. a Caldwell, L. Miyagi, and H.-R. Wenk, *Rev. Sci. Instrum.* 78, 063907  
343 (2007).
- 344 <sup>27</sup> L. Miyagi, W. Kanitpanyacharoen, S.V. Raju, P. Kaercher, J. Knight, A. MacDowell, H.R.  
345 Wenk, Q. Williams, and E.Z. Alarcon, *Rev. Sci. Instrum.* 84, 025118 (2013).
- 346 <sup>28</sup> H.-P. Liermann, S. Merkel, L. Miyagi, H.-R. Wenk, G. Shen, H. Cynn, and W.J. Evans,  
347 *Rev. Sci. Instrum.* 80, 104501 (2009).
- 348 <sup>29</sup> S. Merkel and T. Yagi, *Rev. Sci. Instrum.* 76, 2005 (2005).
- 349 <sup>30</sup> N. Funamori and T. Sato, *Rev. Sci. Instrum.* 79, 1 (2008).
- 350 <sup>31</sup> H.P. Liermann, Z. Konôpková, W. Morgenroth, K. Glazyrin, J. Bednarčík, E.E. McBride,  
351 S. Petitgirard, J.T. Delitz, M. Wendt, Y. Bican, A. Ehnes, I. Schwark, A. Rothkirch, M.  
352 Tischer, J. Heuer, H. Schulte-Schrepping, T. Kracht, and H. Franz, *J. Synchrotron Radiat.* 22,  
353 908 (2015).

- 354 <sup>32</sup> S. Merkel, H.-P. Liermann, L. Miyagi, and H.-R. Wenk, *Acta Mater.* 61, 5144 (2013).
- 355 <sup>33</sup> H. Marquardt, S. Speziale, H.J. Reichmann, D.J. Frost, F.R. Schilling, and E.J. Garnero,  
356 *Science.* 324, 224 (2009).
- 357 <sup>34</sup> J.-F. Lin, H.-R. Wenk, M. Voltolini, S. Speziale, J. Shu, and T.S. Duffy, *Phys. Chem.*  
358 *Miner.* 36, 585 (2009).
- 359 <sup>35</sup> S. Merkel, *J. Geophys. Res.* 107, (2002).
- 360 <sup>36</sup> D. Frost, *Elements* 4, 171 (2008).
- 361 <sup>37</sup> T. Irifune and T. Tsuchiya, in *Treatise Geophys. Second Ed.* (2015).
- 362 <sup>38</sup> K. Kawai and T. Tsuchiya, *Geophys. Res. Lett.* 42, 2718 (2015).
- 363 <sup>39</sup> S.-H. Shim, R. Jeanloz, and T.S. Duffy, *Geophys. Res. Lett.* 29, 2166 (2002).
- 364 <sup>40</sup> R. Caracas, R. Wentzcovitch, G.D. Price, and J. Brodholt, *Geophys. Res. Lett.* 32, 1 (2005).
- 365 <sup>41</sup> D.Y. Jung and A.R. Oganov, *Phys. Chem. Miner.* 32, 146 (2005).
- 366 <sup>42</sup> D.J. Adams and A.R. Oganov, *Phys. Rev. B - Condens. Matter Mater. Phys.* 73, 1 (2006).
- 367 <sup>43</sup> T. Komabayashi, K. Hirose, N. Sata, Y. Ohishi, and L.S. Dubrovinsky, *Earth Planet. Sci.*  
368 *Lett.* 260, 564 (2007).
- 369 <sup>44</sup> T. Uchida, Y. Wang, N. Nishiyama, K. ichi Funakoshi, H. Kaneko, A. Nozawa, R.B. Von  
370 Dreele, M.L. Rivers, S.R. Sutton, A. Yamada, T. Kunimoto, T. Irifune, T. Inoue, and B. Li,  
371 *Earth Planet. Sci. Lett.* 282, 268 (2009).
- 372 <sup>45</sup> M.R. Handy, *J. Struct. Geol.* 16, 287 (1994).
- 373 <sup>46</sup> S. Karato, *Phys. Earth Planet. Inter.* 24, 1 (1981).
- 374 <sup>47</sup> Y.-T. Takeda, *J. Struct. Geol.* 20, 1569 (1998).
- 375 <sup>48</sup> M. Thielmann, G.J. Golabek, and H. Marquardt, *Geochemistry, Geophys. Geosystems* 21, 1  
376 (2020).
- 377 <sup>49</sup> Y. Wang, N. Hilaret, N. Nishiyama, N. Yahata, T. Tsuchiya, G. Morard, and G. Fiquet,  
378 *Geochemistry, Geophys. Geosystems* 14, 3389 (2013).

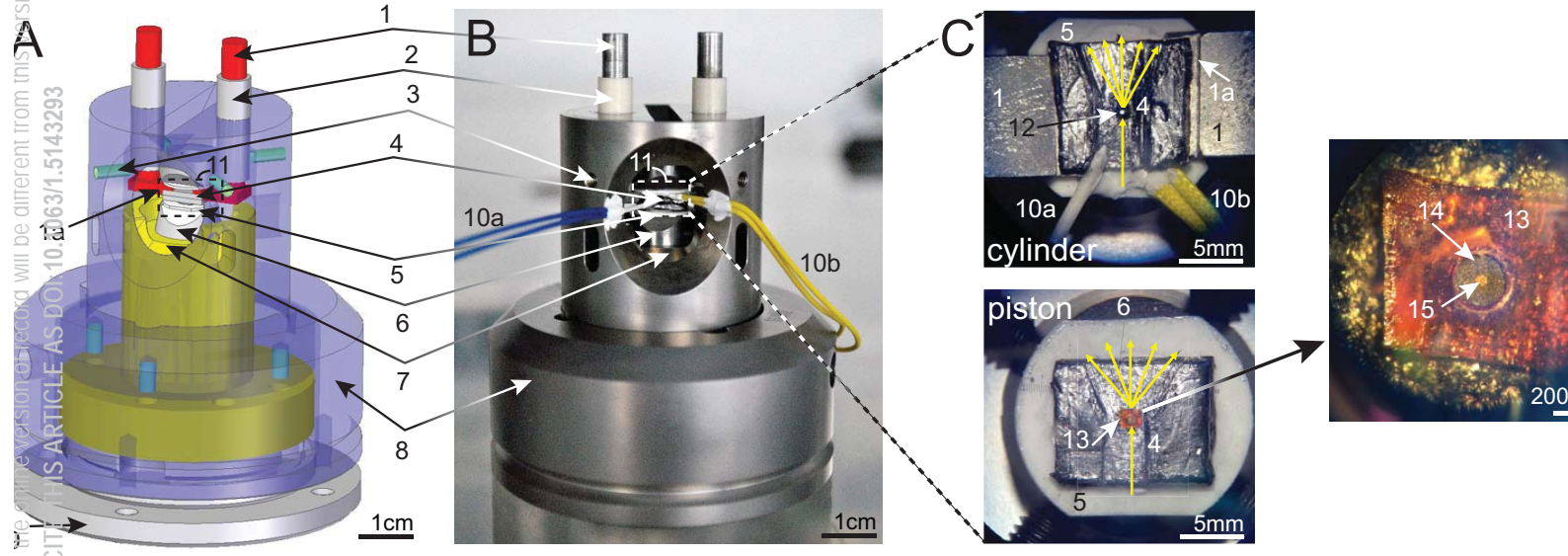
This is the author's peer reviewed, accepted manuscript. However, the online version of record will be different from this version once it has been copyedited and typeset.  
PLEASE CITE THIS ARTICLE AS DOI:10.1063/1.5143293

- 379 <sup>50</sup> P. Kaercher, L. Miyagi, W. Kanitpanyacharoen, E. Zepeda-Alarcon, Y. Wang, F. De Carlo,  
380 and H.-R. Wenk, *Earth Planet. Sci. Lett.* 456, 134 (2016).
- 381 <sup>51</sup> S. Speziale, J. Immoor, A. Ermakov, S. Merkel, H. Marquardt, and H.-P. Liermann, J.  
382 *Appl. Phys.* 126, 105107 (2019).
- 383 <sup>52</sup> Y. Fei, A. Ricolleau, M. Frank, K. Mibe, G. Shen, and V. Prakapenka, *Proc. Natl. Acad.*  
384 *Sci.* 104, 9182 (2007).
- 385 <sup>53</sup> S. Speziale, J. Immoor, A. Ermakov, S. Merkel, H. Marquardt, and H.-P. Liermann, J.  
386 *Appl. Phys.* 126, 105107 (2019).

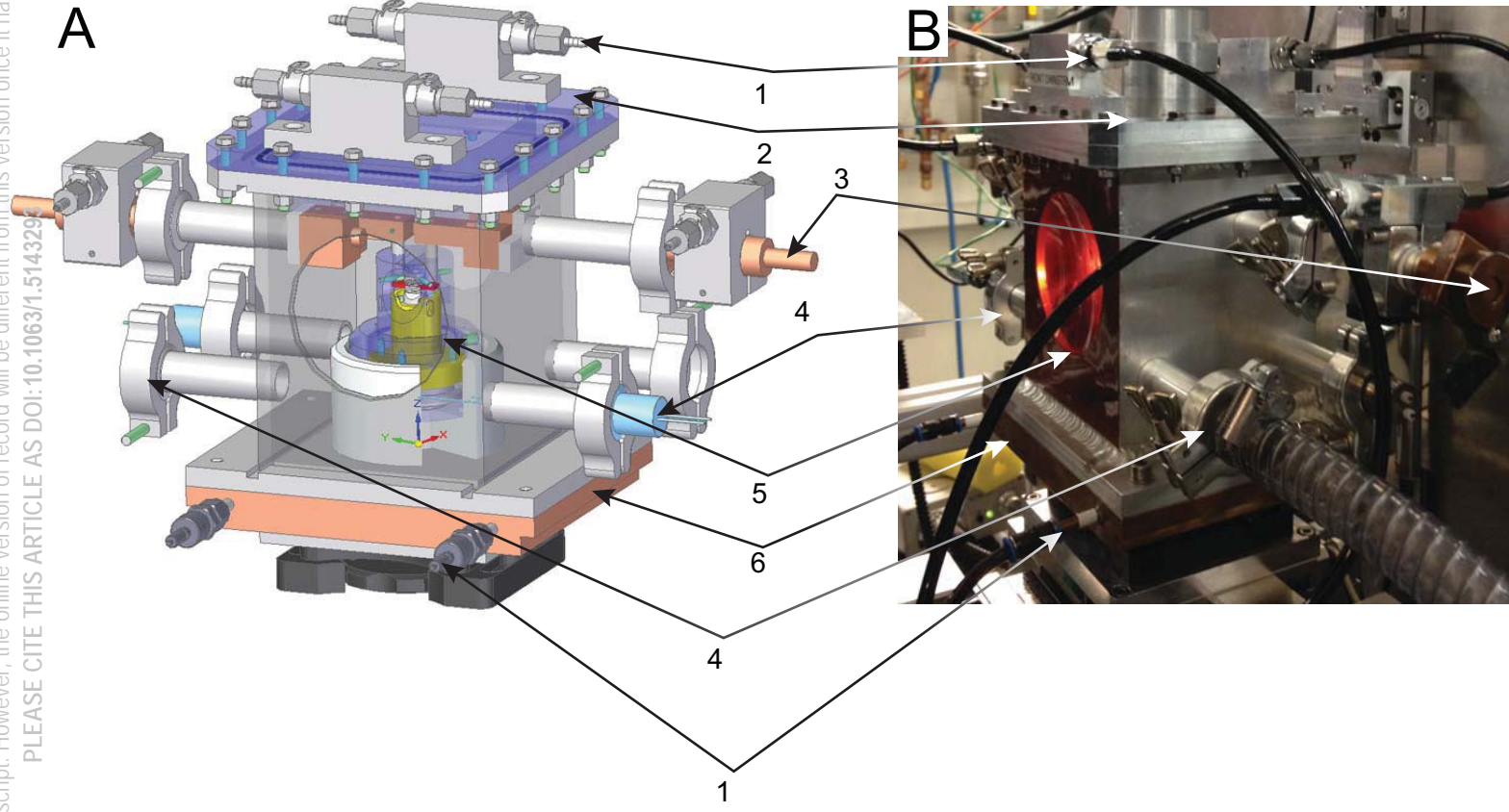
This is the author's peer reviewed, accepted manuscript. However, the online version of record will be different from this version once it has been copyedited and typeset.  
PLEASE CITE THIS ARTICLE AS DOI:10.1063/1.5143293



This is the author's peer reviewed, accepted manuscript. However, the copyright to this article shall be retained by the author(s) and any other rights may be reserved by the copyright owner. This article is intended solely for the personal use of the individual user and is not to be disseminated broadly. This article is subject to the AIP Publishing Terms and Conditions (https://pubs.aip.org/termsandconditions) on AIP Publishing. See the AIP Publishing member benefits (https://pubs.aip.org/member-benefits) for more information. This article is intended solely for the personal use of the individual user and is not to be disseminated broadly. This article is subject to the AIP Publishing Terms and Conditions (https://pubs.aip.org/termsandconditions) on AIP Publishing. See the AIP Publishing member benefits (https://pubs.aip.org/member-benefits) for more information.



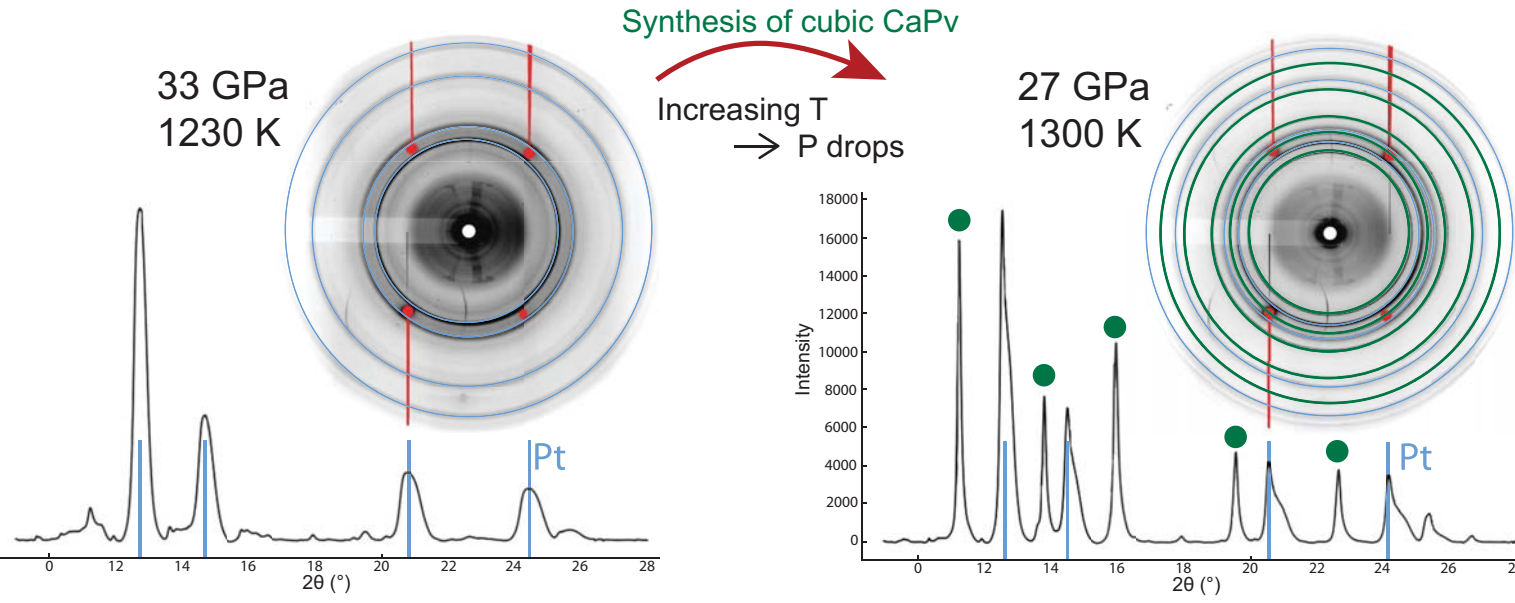
This is the author's peer reviewed, accepted manuscript. However, the online version of record will be different from this version once it has been copyedited and typeset.  
PLEASE CITE THIS ARTICLE AS DOI:10.1063/1.514329



This is the author's peer reviewed, accepted manuscript. However, the online version of this article will be different from this version once it has been copyedited and typeset.

PLEASE CITE THIS ARTICLE AS DOI:10.1119/1.5143293

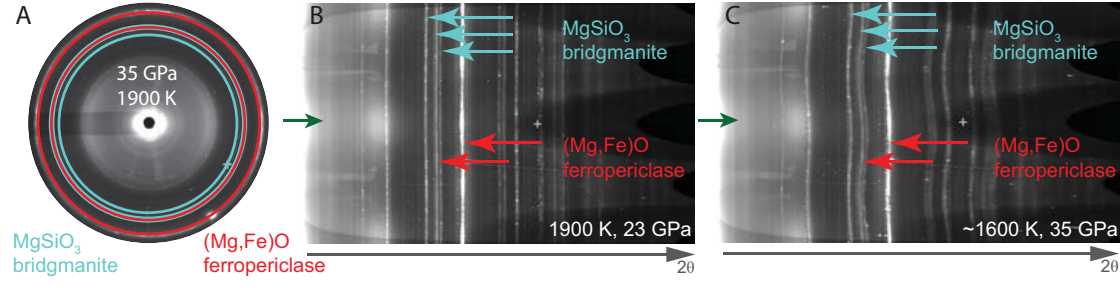
A





This is the author's peer reviewed, accepted manuscript. However, the online version of record will be different from this version once it has been copyedited and typeset.

PLEASE CITE THIS ARTICLE AS DOI:10.1063/1.5143293



This is the author's peer reviewed, accepted manuscript. However, the online version of record will be different from this version once it has been copyedited and typeset.  
PLEASE CITE THIS ARTICLE AS DOI:10.1063/1.5143293

